

Reconstruction of the Jaynes-Cummings field state of ionic motion in a harmonic trapDingshun Lv,¹ Shuoming An,¹ Mark Um,¹ Junhua Zhang,¹ Jing-Ning Zhang,¹ M. S. Kim,^{2,*} and Kihwan Kim^{1,†}¹*Center for Quantum Information, Institute for Interdisciplinary Information Sciences, Tsinghua University, Beijing 100084, People's Republic of China*²*QOLS, Blackett Laboratory, Imperial College London, SW7 2AZ London, England, United Kingdom*

(Received 6 August 2015; published 11 April 2017)

A quantum state is fully characterized by its density matrix or equivalently by its quasiprobabilities in phase space. A scheme to identify the quasiprobabilities of a quantum state is an important tool in the recent development of quantum technologies. One of the most fundamental interaction models in quantum optics is the so-called Jaynes-Cummings model (JCM), which has been massively studied theoretically and experimentally. However, the expected essential dynamics of the field states under the *resonant* JCM has not been observed experimentally due to the lack of a proper reconstruction scheme. In this paper, we further develop a highly efficient vacuum measurement scheme and study the JCM dynamics in a trapped ion system with the capability of the vacuum measurement to reconstruct its quasiprobability Q function, which is a preferred choice to study the core of the dynamics of a quantum state in phase space. During the JCM dynamics, the Gaussian peak of the initial coherent state bifurcates and rotates around the origin of phase space. They merge at the so-called revival time at the other side of phase space. The measured Q function agrees with the theoretical prediction. Moreover, we reconstruct the Wigner function by deconvoluting the Q function and observe the quantum interference in the Wigner function at half of the revival time, where the vibrational state becomes nearly disentangled from the internal energy states and forms a superposition of two composite states. The scheme can be applied to other physical setups including cavity or circuit-QED and optomechanical systems.

DOI: [10.1103/PhysRevA.95.043813](https://doi.org/10.1103/PhysRevA.95.043813)**I. INTRODUCTION**

The Jaynes-Cummings model (JCM) is one of the most fundamental interaction models in quantum mechanics [1], where a single two-level atom resonantly interacts with a single-mode field. The JCM has enabled theoretical and experimental investigations of the basic properties of quantum electrodynamics such as Rabi oscillations of the energy transfer between the two subsystems and collapses and revivals of the oscillations [2]. More recently, the model has been widely studied for its rich properties of quantum control, coherent superposition, and entanglement, which are closely related to the current development of quantum technology. In order to see the nonclassical effects due to quantum interaction, the JCM is often studied with the state initially prepared in a coherent field and the atom in its energy eigenstate. It has been shown that the field and the atom are entangled [3] as soon as the interaction starts, but at a certain time they are nearly disentangled to bring the field into a superposition of two coherent states of a π phase difference [4,5]. Earlier, Eiselt and Risken [6,7] showed that the Gaussian probability distribution of the initial coherent state in phase space breathes at the initial points of interaction, reflecting the Rabi oscillations. Then the Gaussian peak bifurcates to travel around a circle in the opposite direction in phase space. The bifurcation is a consequence of the quantum nature of interaction and was experimentally probed through the measurement of field phase distribution [8,9]. However, the observation of the JCM dynamics by the full reconstruction of the field state has not been experimentally demonstrated.

II. VACUUM MEASUREMENT

Reconstructing the state of a quantum system through measurements reveals all the statistical properties of the system. Thus schemes to reconstruct a quantum state are useful, for example, to ensure the quantum state generated and to test the fidelity of quantum operations. The quantum state is equivalently represented by its density matrices or quasiprobability functions in phase space [10]. Among the quasiprobability functions, the Wigner function has been used mainly for the study of nonclassicality of the state, which is manifested by negativities [11]. The Q function has been used to study the essence of the dynamics of a quantum-state evolution in phase space [3–9,12–15]. Recently, there have been many developments in reconstructing the state of a quantum field in various physical systems including photonic systems [16,17], atomic systems [18], molecular systems [19], cavity QED [20], circuit-QED systems [21,22], and trapped-ion systems [23–26], which are mostly related to the reconstruction of Wigner functions by the parity measurements of the states. For the reconstruction of the Wigner function in trapped-ion systems, all the phonon number distributions in the Fock state basis [23] or in the displaced basis [24] are used. Alternatively, the direct parity measurements through nonlinear coupling to another motional mode [25] or internal level [26] are applied.

The Q function allows one to study the core of the dynamics of a quantum state in phase space and has been a preferred choice of study theoretically [3–7] and experimentally [8,9,13–15]. The definition of the Q function is $Q(\alpha) = \frac{1}{\pi} \langle 0 | \hat{D}^\dagger(\alpha) \hat{\rho} \hat{D}(\alpha) | 0 \rangle$, where $\hat{D}(\alpha)$ is the displacement operator [27]. The value of the Q function is merely the weight of the vacuum component of a given state once it is displaced in phase space by α , which looks relatively easy to implement. The reconstruction of the Q function also does not

*m.kim@imperial.ac.uk

†kimkihwan@gmail.com

require a heavy numerical process as the probability of the state being in the vacuum is the value of the Q function in each point of phase space. However, the measurement of the vacuum state is not straightforward. In a cavity, as an example, the existence of a photon can be detected by an atomic state through an atom-photon interaction like JCM [1]. If the cavity has no photons, an atom initially prepared in its ground state will remain there forever. However, by merely measuring the atom in its ground state we cannot say that the cavity is empty because the Rabi oscillations periodically bring the atom back to the ground state even with many photons in the cavity. The oscillation frequency depends on how many photons are present in the cavity. The authors in Refs. [8,9,13,28] demonstrated a scheme of vacuum measurement that works for their particular cavity-QED system. For the circuit-QED system [15], a measurement of the vacuum component and the Q -function reconstruction was demonstrated based on the system-specific strong nonlinear coupling between the cavity mode and the artificial atom. Recently a generic scheme of the vacuum measurement was proposed for the cavity-QED system with the standard JCM coupling [29].

While it is desirable to find the Q function and the Wigner function based on one set of measurements, this has not been achieved due to the measurement inefficiencies of the vacuum state. Here, we report a generic and efficient detection of vacuum with 98.5 (± 0.3)% efficiency for the phononic states in the vibrational mode of a harmonic trap, which is realized by the adiabatic passage schemes [30,31] based on counterdiabatic methods [32–34]. The efficiency of 98.5 (± 0.3)% is the probability of detecting the vacuum state when the phonon is prepared in the vacuum state, which is mainly limited by the discrimination efficiency of the internal state. We obtain the efficiency by repeating 10 000 times the measurements after preparing the vacuum state and counting the number of events that detect no fluorescences. The probability of assigning the vacuum state even if the ion is not in the vacuum state is 1.0 (± 0.3)%. The demonstrated adiabatic passages were used for deterministically adding and subtracting single phonons in the range of less than six phonons [31]. The adiabatic passages have been significantly improved to cover much higher phonon number states up to $\langle n \rangle \sim 25$, which allow us to measure the vacuum components in a relatively large area $|\alpha| \leq 3$ in phase space. To make such improvements, we carefully optimize all the experimental parameters of the adiabatic passages. In particular, we find the optimal laser intensity to enhance the performance of the uniform transfer for the large phonon number states.

Typically, in trapped-ion systems, phonon number distributions are measured by the Fourier transformation of the phonon-number dependent Rabi oscillations [35–37]. For this, it is necessary to observe multiple detailed oscillations of the internal state under the JCM interaction, which requires a long data-taking time. Our scheme does not require such a long observation, but a single measurement, and we obtain a binary result: the vacuum or the complementary states. Practically, the actual time to obtain the Q function is reduced by more than 20 times. We simply need to repeat the measurement sequence for the probabilities of the vacuum state, which by the nature of the measurement excludes the negativity problem from experimental error. We efficiently measure the vacuum

probabilities in phase space to observe the dynamics of the JCM field. The measured Q function is highly accurate, which enables us to reconstruct the density matrix and the Wigner function by its deconvolution. We show a good agreement of our quasiprobabilities with the theoretical predictions.

III. EXPERIMENTAL SCHEME

A. Experimental setup

We employ the vibrational mode of a single trapped ion $^{171}\text{Yb}^+$ in a harmonic potential with the frequency of $\omega_X = (2\pi)2.8$ MHz. We encode the qubit state into two hyperfine states $|F = 1, m_F = 0\rangle \equiv |\uparrow\rangle$ and $|F = 0, m_F = 0\rangle \equiv |\downarrow\rangle$ of the $S_{1/2}$ manifold with the transition frequency $\omega_{\text{HF}} = (2\pi)12.6428$ GHz. We perform the experimental demonstration by the usage of Raman laser beams, which are generated by the frequency-doubled mode-locked picosecond-pulse laser with repetition rate 76.22 MHz and a central wavelength of 375.5 nm. The laser beam is split into two paths, sent through two acousto-optic modulators (AOMs), and then focused on the ion's position. The AOMs are used for the control of frequencies and amplitudes of the Raman laser beams. In the experiments, we fix the frequency and amplitude of one AOM, and we only control those parameters of the other AOM for the necessary operations. The pulse durations of the laser beams are precisely controlled by the field programmable gate array.

B. Realization of Jaynes-Cummings model

We realize the JCM or anti-JCM by applying a pair of counterpropagating Raman beams that have the frequency differences of $(\omega_{\text{R1}} - \omega_{\text{R2}}) = \omega_{\text{HF}} \mp \omega_X$, respectively, as shown in Fig. 1(a). In the interaction picture, the Raman laser interactions can be described by the following JCM and anti-JCM Hamiltonians:

$$\begin{aligned}\hat{H}_{\text{JCM}}(\phi) &= \frac{\hbar\eta\Omega}{2}(\hat{a}\hat{\sigma}_+e^{i\phi} + \hat{a}^\dagger\hat{\sigma}_-e^{-i\phi}), \\ \hat{H}_{\text{aJCM}}(\phi) &= \frac{\hbar\eta\Omega}{2}(\hat{a}^\dagger\hat{\sigma}_+e^{i\phi} + \hat{a}\hat{\sigma}_-e^{-i\phi}).\end{aligned}\quad (1)$$

Here, \hat{a}^\dagger and \hat{a} are the phonon creation and annihilation operators, $\hat{\sigma}_+(\hat{\sigma}_-) = |\uparrow\rangle\langle\downarrow|$ ($|\downarrow\rangle\langle\uparrow|$) is the spin-raising (lowering) operator, Ω is the vacuum Rabi frequency of (anti-)JCM, $\eta = \Delta k\sqrt{\hbar}/M\omega_X$ is the Lamb-Dicke parameter with Δk the net wave vector of the Raman laser beams, M is the mass of the $^{171}\text{Yb}^+$ ion, and ϕ is the phase difference of the Raman laser beams. As shown in Eq. (1) the JCM and anti-JCM models of the field state are equivalent; for instance, by exchanging the internal states $|\downarrow\rangle$ with $|\uparrow\rangle$ in the interpretation, the dynamics of the two models are the same. For technical reasons, we perform experiments for the anti-JCM interaction.

C. Implementation of the state-independent displacement operation

When the beat-note frequency of Raman beams $(\omega_{\text{R1}} - \omega_{\text{R2}})$ is equal to the trap frequency ω_X as shown in the middle panel of Fig. 1(a), the effective Hamiltonian in the interaction

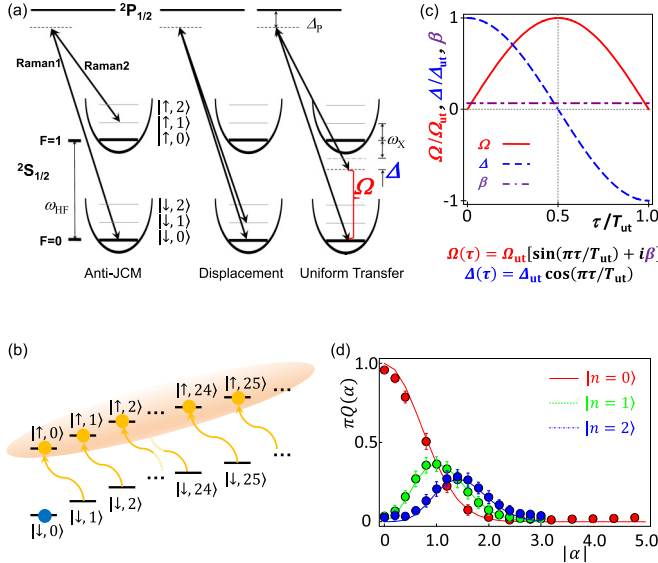


FIG. 1. Raman laser schemes and the vacuum measurement. (a) The Hilbert space of the system is composed of the direct product of qubit states $\{|\downarrow\rangle, |\uparrow\rangle\}$ and phonon number states $\{|n=0\rangle, |1\rangle, |2\rangle, \dots\}$. Raman laser beams, which have σ_- polarization and are detuned by $\Delta_p \approx 12.9$ THz from the $P_{1/2}$ manifold, perform anti-JCM, displacement operation, and the vacuum measurement by adjusting their beating frequencies. (b) The vacuum component is measured by transferring the population of $|\downarrow, n\rangle$ to that of $|\uparrow, n-1\rangle$ for any value of n at the same duration of pulse. The atom remaining in no fluorescence state $|\downarrow\rangle$ indicates the phononic state being in $|0\rangle$. (c) The uniform transfer for any phononic state $|n\rangle$ to $|n-1\rangle$ is accomplished by the scheme of shortcuts to the adiabaticity, where $\Omega_{\text{ut}} = (2\pi)22.7$ kHz, $\beta = 0.075$, $\Delta_{\text{ut}} = 1.9\Omega_{\text{ut}}$, and the total duration $T_{\text{ut}} = 198.2$ μs . (d) Q function of phononic Fock state $n = 0, 1, 2$ depending on the amount of displacement $|\alpha|$. The points with error bars are the experimental results while the dashed lines are by the theory. The error bars are obtained by the standard deviation of the quantum projection noise with 100 repetitions.

picture is described by [31]

$$\hat{H}_D = \frac{i\hbar\Omega_D}{2}(\hat{a}^\dagger e^{i\phi} + \hat{a}e^{-i\phi}), \quad (2)$$

where Ω_D is the Rabi frequency and ϕ is the relative phase of the two Raman laser beams. The application of the Hamiltonian (2) performs the displacement operation $\hat{D}(\alpha) = e^{\alpha\hat{a}^\dagger - \alpha^*\hat{a}}$, where $\alpha = i\eta\Omega_D t/2$.

The displacement operation is near-equally performed for both qubit states $\{|\downarrow\rangle, |\uparrow\rangle\}$ due to the large detuning $\Delta_p \approx -(2\pi)12.9$ THz of the Raman beams from the ${}^2P_{1/2}$ level. The difference in the strength Ω_D between $|\downarrow\rangle$ and $|\uparrow\rangle$ can be written as $\frac{g^2}{2\Delta_p} - \frac{g^2}{2(\Delta_p + \omega_{\text{HF}})} \approx \frac{g^2}{2\Delta_p} \frac{\omega_{\text{HF}}}{\Delta_p}$, where g is the Rabi frequency of each Raman beam coupled to the transition ${}^2S_{1/2} \leftrightarrow {}^2P_{1/2}$ and $\frac{g^2}{2\Delta_p} \approx \Omega_D$. Therefore, the strength difference should be less than $\frac{\omega_{\text{HF}}}{\Delta_p} \approx 10^{-3}$.

D. Efficient vacuum measurement

The essence of the vacuum-component measurement is in the realization of the uniform population transfer of

$|\downarrow, n\rangle \rightarrow |\uparrow, n-1\rangle$ for any n as shown in Fig. 1(b). After the uniform transfer, all the phonon states except the vacuum component $|n=0\rangle$ are in the bright electronic state $|\uparrow\rangle$, which emits photons during the standard fluorescence detection sequence. Therefore, the atom being in the dark electronic state $|\downarrow\rangle$ after the uniform transfer indicates the phonon state in the vacuum. By measuring the vacuum probability of the state after displacing it by α , we can directly measure the Q function $Q(\alpha)$.

In general, the frequency of the Rabi oscillations between $|\downarrow, n\rangle$ and $|\uparrow, n-1\rangle$ has \sqrt{n} dependency due to the nature of JCM coupling. To accomplish the uniform transfer, we basically apply an adiabatic passage, but in much shorter time than what is required for the adiabatic evolution—the so-called shortcuts to adiabaticity [30–34]. We note that in trapped-ion experiments similar rapid adiabatic passages have been used for manipulation of electronic state [38], investigation of cooling dynamics, [39] and estimation of the temperature [40]. Here, as shown in Fig. 1(c), the detuning $\Delta \equiv (\omega_{R1} - \omega_{R2}) - (\omega_{\text{HF}} - \omega_X)$ and the amplitude Ω of Raman laser beams are swept by $\Delta(t) = \Delta_{\text{ut}} \cos(\pi t/T_{\text{ut}})$ and $\Omega(t) = \Omega_{\text{ut}}[\sin(\pi t/T_{\text{ut}}) + i\beta]$, where $i\beta$ is the counterdiabatic field that is applied at a constant amplitude 90 deg out of phase with the driving field to suppress excitations during the fast evolution [30–34]. The value of the counterdiabatic parameter β is experimentally optimized [31]. We generate the complex waveform through the arbitrary waveform generator. We evaluate the reliability of the uniform transfer by performing the Q -function measurements for the phonon number states $|n=0, 1, 2\rangle$ as shown in Fig. 1(d). Here, we prepare the phonon number states $|n=0, 1, 2\rangle$ and displace them along one direction in phase space. We note that we do not observe serious deviation from zero over the error bar in the values of Q -function measurements as the displacements increase to around 4.8 as shown in Fig. 1(d).

IV. RESULTS AND DISCUSSIONS

A. Q -function reconstruction for JCM dynamics

It was found that the atom and the field in the JCM or anti-JCM are nearly disentangled during the course of interaction if the atom is initially prepared in a superposition of $|\uparrow\rangle$ and $|\downarrow\rangle$ and the field is initially in the coherent state $|\alpha\rangle$ of its amplitude α with $|\alpha| \gg 1$ [41]. Let us consider the initial state of the atom $|\Psi_A^\pm\rangle = (|\uparrow\rangle \mp i|\downarrow\rangle)/\sqrt{2}$. By the interaction (1), the atom-field state evolves to $|\Psi_{A-P}^\pm(t)\rangle = |\Psi_P^\pm(t)\rangle \otimes |\Psi_A^\pm(t)\rangle$ [41], where

$$|\Psi_A^\pm(t)\rangle = (e^{\pm i\pi t/t_{\text{rev}}} |\downarrow\rangle \mp i|\uparrow\rangle)/\sqrt{2}, \quad (3)$$

$$|\Psi_P^\pm(t)\rangle = \exp\left(\mp it \frac{\eta\Omega\sqrt{\hbar}}{2}\right) |\alpha e^{\pm i\pi t/t_{\text{rev}}}\rangle. \quad (4)$$

From this, it is clear that if the atom is prepared in its ground state $|\downarrow\rangle$ $[=(|\Psi_A^-) - |\Psi_A^+)]/\sqrt{2}i]$ the atom-phonon state will be in the superposition of $|\Psi_{A-P}^\pm(t)\rangle$. The phonon state will rotate in phase space, where $t_{\text{rev}} = \frac{4\pi|\alpha|}{\eta\Omega}$ is the corresponding revival time.

In the experiments, we prepare a coherent state of $\beta = 1.62(0.05)$ with the internal state $|\downarrow\rangle$ by displacing the $|n=0\rangle$

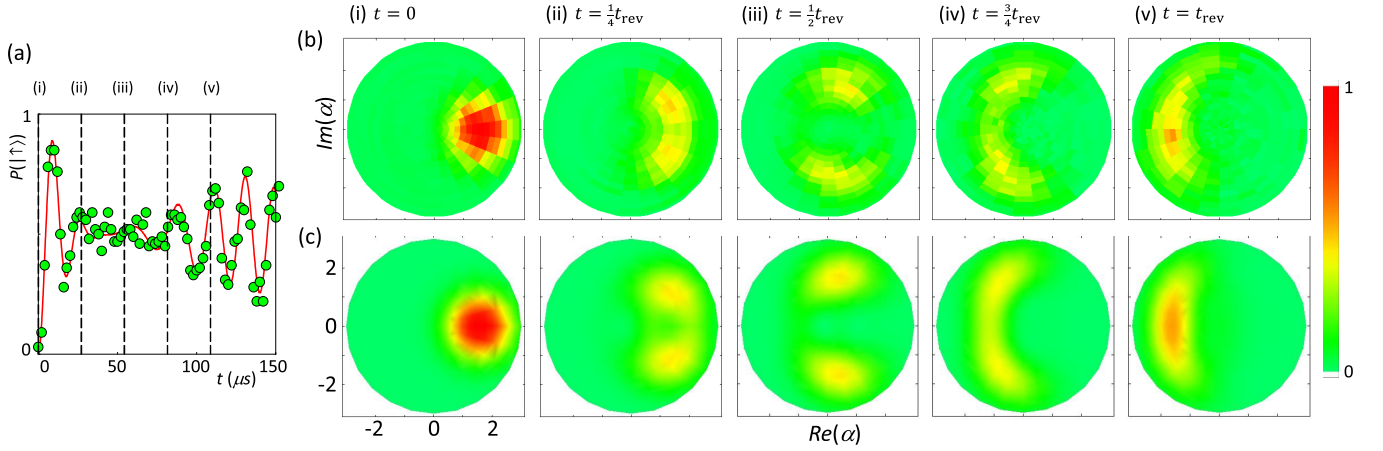


FIG. 2. The time evolution of the Q function for an initial coherent state under anti-JCM interaction. (a) Collapse and revival of the Rabi oscillation signal and (b) experimentally measured and (c) numerically calculated Q functions of the phonon field with the initial coherent state $|\beta = 1.62(0.05)\rangle$ depending on the duration of anti-JCM interaction. (a) $P(|\uparrow\rangle)$ is the probability of detecting the atom in $|\uparrow\rangle$. The points are obtained after 100 repetitions. The solid line is from fitting the data with $\sum_{n=0} \frac{1}{2} [1 - e^{-\gamma t} \cos(\sqrt{n+1}\eta\Omega t)]$, where γ is the empirical decay constant. At (b) and (c), the time for each snapshot of the Q functions are labeled as (i)–(v) in the unit of the revival time t_{rev} , where $t_{\text{rev}} = \frac{4\pi|\alpha|}{\eta\Omega} = 108.8 \mu\text{s}$. In (b), each Q function is obtained from 100 repetitions of the vacuum measurements after 384 different displacements, where the amplitude and the phase of displacement $|\alpha|e^{i\varphi}$ are scanned from zero to 3.0 with the step size of 0.2 and from zero to 2π with the 24 steps, respectively.

state after the standard Raman-sideband ground-state cooling. Then we apply Raman laser beams for the anti-JCM interaction and observe the dynamics of the atom and the field. For the internal state of the atom, we measure the probability of being in the $|\uparrow\rangle$ state, $P(|\uparrow\rangle)$ by the standard fluorescence detection scheme. For the field, we choose five different interaction times $t = (0, \frac{1}{4}, \frac{1}{2}, \frac{3}{4}, 1)t_{\text{rev}}$ in the anti-JCM. After the interaction time t , we displace the state by α and trace over the internal degree of freedom by the standard optical pumping sequence, which does not produce any noticeable change of the phonon distribution as shown in Fig. 3(a). Then we measure the vacuum component to reconstruct $Q(\alpha)$. We note that we observe that the essence of the dynamics remains largely the

same, though the amplitude of the initial coherent state is not much larger than 1.

Figures 2(b) and 2(c) show the experimental and theoretical time evolution of the initial coherent state under the anti-JCM interaction. The theoretical results are obtained by the numerical simulation of the master equation of the anti-JCM Hamiltonian including experimental imperfections [30]. At $t = 0$, $P(|\uparrow\rangle) = 0$ and $Q(\alpha)$ is Gaussian, which represents the coherent state. At time $t = t_{\text{rev}}/4$, while the Rabi oscillations begin to collapse, the Gaussian peak splits into two, which can be understood by the separation of two atom-phonon states $|\Psi_{A-P}^{\pm}\rangle$. The two components of the atom-phonon entangled state evolve in the opposite phases as shown in Eqs. (3) and (4). At the half-revival time $t = t_{\text{rev}}/2$, the two atomic states in Eq. (3) become identical except the global phase, which results in disentanglement of the atomic state from the phonon state (see also Fig. 5). In the Q function, the phonon state shows two clearly separated peaks that are located at the opposite phases in phase space. This can be understood as the superposition of two coherent states [41]. Note that the bigger the initial coherent state the more obvious the splitting. Further evolution of the phonon state is shown in Figs. 2(iv) and 2(v). At the revival time $t = t_{\text{rev}}$, the two phonon peaks merge at the opposite position of the initial coherent state, which causes the revival of the Rabi oscillations as shown in Fig. 3(b). Due to the quadratic phase term in Eq. (4), the amplitude of the Rabi oscillations is reduced.

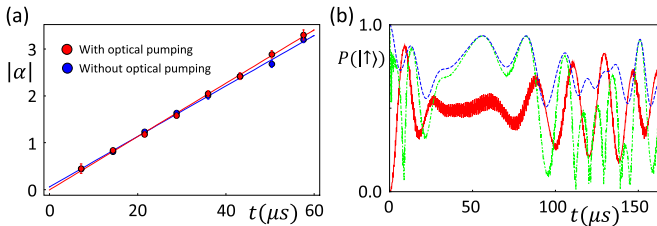


FIG. 3. (a) Test of the influence of the optical pumping sequence to the phonon number distribution. The coherent states prepared in $|\downarrow\rangle$ state (red circles) are compared with those prepared in $|\uparrow\rangle$ state by an optical pumping pulse (blue circles). The amount of the displacement $|\alpha|$ is measured by coherent-state fitting to the phonon number distribution. (b) The relation between Rabi contrast, purity, and atomic coherence. The red curve is the Rabi oscillation signal, the blue dashed line is the purity of the phononic state, and the green dot-dashed line is the atomic coherence, the absolute value of the off-diagonal elements of the atomic density matrix after tracing over the phononic field state. All curves are obtained by the numerical calculations.

B. Time-reversal operation

In order to confirm the whole dynamics keeping coherence, we perform the time-reversal operation, which forces the phonon state evolved under the anti-JCM interaction to retrace its past trajectory in the opposite direction by the generalized echo scheme [42]. For the echo method, we introduce a π phase shift in the second half of the anti-JCM interaction, i.e.,

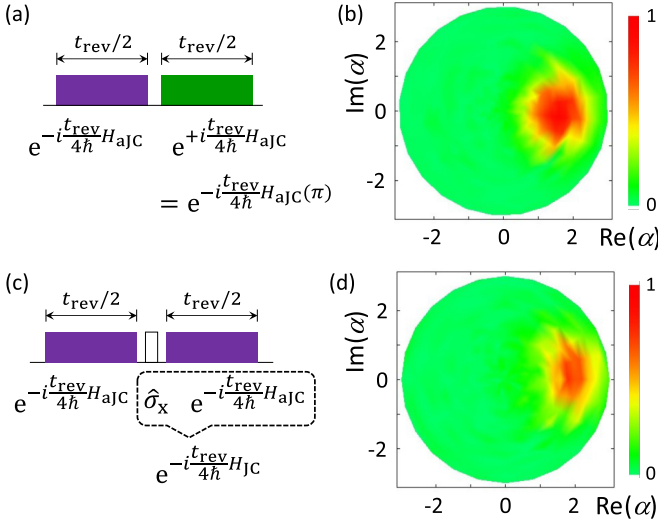


FIG. 4. (a) Generalized echo-sequence time reversal of anti-JCM evolution for the interaction time $t = t_{\text{rev}}/2$. The $\phi = \pi$ phase of the anti-JCM Hamiltonian produces the negative sign; $H_{\text{ajc}}(\pi) = -H_{\text{ajc}}(0)$, which performs the time-reversal operation. (b) The measured Q function of the phononic state after time-reversal operation of (a). (c) JCM sequence for the time reversal of anti-JCM evolution for the interaction time $t = t_{\text{rev}}/2$. The JCM coupling is realized by a σ_x pulse and the anti-JCM coupling. The phase $\frac{\pi}{2}$ of the second anti-JCM pulse is chosen to maximize the fidelity of the reverse operation. (d) Measured Q function of the phononic state after the reversal operation. The total number of measurements for the Q -function reconstruction is the same as that in Fig. 2.

$e^{-i \frac{t}{2\hbar} H_{\text{ajc}}(\pi)} = e^{+i \frac{t}{2\hbar} H_{\text{ajc}}}$. The process is called time reversal as in Ref. [43]. We apply the reverse process at the half-revival time $t = t_{\text{rev}}/2$ and observe that the state is brought back to the initial coherent state at the time $t = t_{\text{rev}}$ with the fidelity of 0.914(4) through the Q -function measurement shown in Figs. 4(a) and 4(b). Since keeping the coherence of the interaction is at the heart of the time reversal, our result of time reversal clearly confirms that the process occurs in the quantum regime. We also study another way of reversing the anti-JCM by applying the JCM as shown in Figs. 4(c) and 4(d) [44].

C. Wigner function reconstruction from Q function

In addition to the time-reversal process, we demonstrate the coherence property by detecting nonclassicality generated during the evolution, in particular, interferences of the composite states of the two peaks in phase space. For this purpose, we reconstruct the Wigner function from our measured Q function. We first find the density matrix by deconvoluting the Q function by the convex optimization and reconstruct the Wigner function from the density matrix. The relation between the Q function and the density matrix is described as

$$\begin{aligned} Q(\alpha) &= \frac{1}{\pi} \langle \alpha | \rho | \alpha \rangle \\ &= \frac{1}{\pi} \sum_{n=0}^{n_{\text{max}}} \sum_{m=0}^{n_{\text{max}}} \langle \alpha | n \rangle \langle n | \rho | m \rangle \langle m | \alpha \rangle \end{aligned}$$

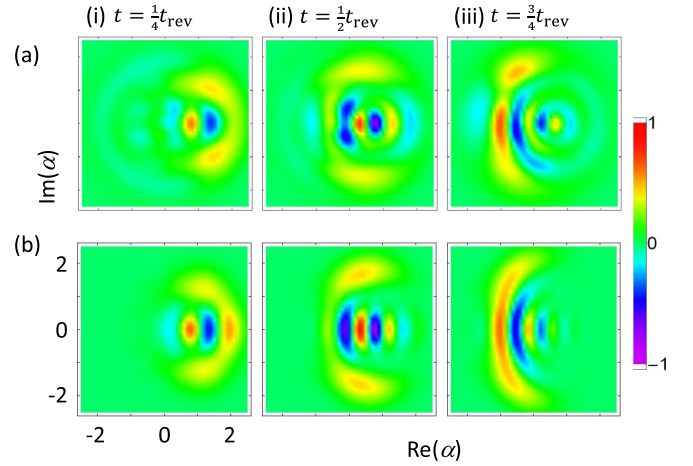


FIG. 5. The Wigner function reconstruction from the Q function at various times of the anti-JCM evolution, $t = \frac{1}{4}, \frac{1}{2}, \frac{3}{4} t_{\text{rev}}$. The negativities of the Wigner functions indicate the emergence of the nonclassical state during the dynamic evolution. (a) The Wigner functions are reconstructed from the density matrix obtained by deconvoluting the experimentally measured values of the Q functions shown in Fig. 2(b). The density matrices are reconstructed by deconvoluting the Q functions with the convex optimization. We note that we use the data $|\alpha| \leq 1$ for the optimum fidelity and it is necessary to use proper initial guess of the density matrix for the convergence of the deconvolution. (b) The Wigner functions are directly obtained by the numerical calculation of the anti-JCM dynamics.

$$= \frac{e^{-|\alpha|^2} \alpha^m (\alpha^*)^n}{\pi \sqrt{m!n!}} \sum_{n=0}^{n_{\text{max}}} \sum_{m=0}^{n_{\text{max}}} \rho_{n,m}, \quad (5)$$

where n_{max} is the maximum phonon number that we include for the reconstruction. With the sufficient number of measured values of the Q function over $n_{\text{max}} \times n_{\text{max}}$, we can inverse the multiple equations of Eq. (5) and reconstruct the density-matrix elements. Mainly due to the quantum projection noise in the measurements, however, the direct inverse of the equations may result in unphysical results including the negativity of the diagonal components in the density matrix. In order to avoid the problem, we apply a method of convex optimization of least-square function with constraints. Here we first define a function F as follows:

$$\begin{aligned} F &= \sum_{i=0}^{i_{\text{max}}} |Q^{\text{exp}}(\alpha_i) - Q^{\text{rec}}(\alpha_i)|^2 \\ &= \sum_{i=0}^{i_{\text{max}}} \left| Q^{\text{exp}}(\alpha_i) - \frac{e^{-|\alpha_i|^2} \alpha_i^m (\alpha_i^*)^n}{\pi \sqrt{m!n!}} \sum_{n=0}^{n_{\text{max}}} \sum_{m=0}^{n_{\text{max}}} \rho_{n,m} \right|^2 \end{aligned} \quad (6)$$

where $Q^{\text{exp}}(\alpha_i)$ and $Q^{\text{rec}}(\alpha_i)$ are the experimentally measured and the numerically reconstructed Q functions, respectively, at α_i in phase space, and i_{max} is the maximum number of displacements involved to construct the density matrix. Then we minimize the function F under the constraints of the density matrix, which should be positive semidefinite of trace 1. Note that we find the convergence of the minimization algorithm depends on the choice of the state of initial guess.

Figure 5(a), which is reconstructed from the experimental data of the Q -function measurement, clearly manifests inter-

ference patterns of the composite states at the half-revival time and negativities in other interaction times. The experimental reconstruction of the Wigner function of Fig. 5(a) is in good agreement with the direct theoretical reconstruction of the Wigner function shown in Fig. 5(b). We also obtain the purities $\text{Tr}(\rho^2)$ of the states from the experimentally reconstructed density matrix. At $t = t_{\text{rev}}/2$, the purity is 0.82(0.05), which indicates the phonon state is not entirely pure, possibly because of its entanglement with the internal state [see Fig. 3(b)]. Theoretical studies [4] suggest that the purity ideally reaches unity as the size of the initial coherent state increases.

V. CONCLUSION

We have shown a highly efficient scheme to detect the vacuum which is used to reconstruct the dynamics of the JCM field state. The efficient measurement of the Q function enables us to reconstruct the Wigner function, offering a demonstration of the Wigner function reconstruction from the vacuum measurement. Our developed technique of the Q -function measurement can be used to probe other dynamics of the phonon field including Kerr dynamics. In our experimental demonstration, the size of the initial coherent state $|\beta\rangle$ could be increased by improving the ion trap system.

The main limitation of the current demonstration comes from the unreliable displacement operation above $\alpha \approx 4.8$, which is caused by the heating of the phonon mode and going outside the Lamb-Dicke regime of the phonon state. We may reach an order-of-magnitude large phonon number state by the reduction of an order of magnitude in the heating rate together with making the Lamb-Dicke parameter three times smaller by changing the configuration of Raman beams. Our approach is generic and would also be applied to other physical platforms that have a Jaynes-Cummings type of coupling including optomechanics and circuit-QED systems.

ACKNOWLEDGMENTS

This work was supported by the National Key Research and Development Program of China under Grants No. 2016YFA0301900 and No. 2016YFA0301901 and the National Natural Science Foundation of China Grants No. 11374178, No. 11574002, and No. 11504197. M.S.K. thanks Matteo Paris, Girish Agarwal, and Werner Vogel for the discussions on the Wigner function reconstruction and was supported by the Engineering and Physical Sciences Research Council (Grant No. EP/K034480/1) and the Royal Society.

-
- [1] E. T. Jaynes and F. W. Cummings, *Proc. IEEE* **51**, 89 (1963).
 - [2] J. H. Eberly, N. B. Narozhny, and J. J. Sanchez-Mondragon, *Phys. Rev. Lett.* **44**, 1323 (1980).
 - [3] S. P. D. Phoenix and P. L. Knight, *Ann. Phys.* **186**, 381 (1988).
 - [4] J. Gea-Banaclache, *Phys. Rev. Lett.* **65**, 3385 (1990).
 - [5] J. Gea-Banaclache, *Phys. Rev. A* **44**, 5913 (1991).
 - [6] J. Eiselt and H. Risken, *Opt. Commun.* **72**, 351 (1989).
 - [7] J. Eiselt and H. Risken, *Phys. Rev. A* **43**, 346 (1991).
 - [8] A. Auffeves, P. Maioli, T. Meunier, S. Gleyzes, G. Nogues, M. Brune, J.-M. Raimond, and S. Haroche, *Phys. Rev. Lett.* **91**, 230405 (2003).
 - [9] J.-M. Raimond, T. Meunier, P. Bertet, S. Gleyzes, P. Maioli, A. Auffeves, G. Nogues, M. Brune, and S. Haroche, *J. Phys. B* **38**, S535 (2005).
 - [10] K. E. Cahill and R. J. Glauber, *Phys. Rev.* **177**, 1882 (1969).
 - [11] A. Kenfack and K. Życzkowski, *J. Opt. B* **6**, 396 (2004).
 - [12] J. F. Poyatos, R. Walser, J. I. Cirac, P. Zoller, and R. Blatt, *Phys. Rev. A* **53**, R1966 (1996).
 - [13] J.-M. Raimond and S. Haroche, *Exploring the Quantum* (Oxford University Press, Oxford, 2006).
 - [14] M. Greiner, O. Mandel, T. W. Hänsch, and I. Bloch, *Nature (London)* **419**, 51 (2002).
 - [15] G. Kirchmair, B. Vlastakis, Z. Leghtas, S. E. Nigg, H. Paik, E. Ginossar, M. Mirrahimi, L. Frunzio, S. M. Girvin, and R. J. Schoelkopf, *Nature (London)* **495**, 205 (2013).
 - [16] D. T. Smithey, M. Beck, M. G. Raymer, and A. Faridani, *Phys. Rev. Lett.* **70**, 1244 (1993).
 - [17] A. I. Lvovsky and M. G. Raymer, *Rev. Mod. Phys.* **81**, 299 (2009).
 - [18] C. Kurtsiefer, T. Pfau, and J. Mlynek, *Nature (London)* **386**, 150 (1997).
 - [19] T. J. Dunn, I. A. Walmsley, and S. Mukamel, *Phys. Rev. Lett.* **74**, 884 (1995).
 - [20] S. Deleglise, I. Dotsenko, C. Sayrin, J. Bernu, M. Brune, J.-M. Raimond, and S. Haroche, *Nature (London)* **455**, 510 (2008).
 - [21] M. Hofheinz, H. Wang, M. Ansmann, R. C. Bialczak, E. Lucero, M. Neeley, A. D. O'Connell, D. Sank, J. Wenner, J. M. Martinis *et al.*, *Nature (London)* **459**, 546 (2009).
 - [22] B. Vlastakis, G. Kirchmair, Z. Leghtas, S. E. Nigg, L. Frunzio, S. M. Girvin, M. Mirrahimi, M. H. Devoret, and R. J. Schoelkopf, *Science* **342**, 607 (2013).
 - [23] D. Leibfried, D. M. Meekhof, B. E. King, C. Monroe, W. M. Itano, and D. J. Wineland, *Phys. Rev. Lett.* **77**, 4281 (1996).
 - [24] D. Kienzler, C. Flühmann, V. Negnevitsky, H.-Y. Lo, M. Marinelli, D. Nadlinger, and J. P. Home, *Phys. Rev. Lett.* **116**, 140402 (2016).
 - [25] S. Ding, G. Maslennikov, R. Hablutzel, H. Loh, and D. Matsukevich, *arXiv:1512.01670*.
 - [26] A. Noguchi, K. Toyota, and S. Urabe (private communication).
 - [27] S. Barnett and P. M. Radmore, *Methods in Theoretical Quantum Optics* (Oxford University Press, Oxford, 1997).
 - [28] A. Signoles, A. Facon, D. Grosso, I. Dotsenko, S. Haroche, J.-M. Raimond, M. Brune, and S. Gleyzes, *Nat. Phys.* **10**, 715 (2014).
 - [29] D. K. L. Oi, V. Potocěk, and J. Jeffers, *Phys. Rev. Lett.* **110**, 210504 (2013).
 - [30] S. An, J.-N. Zhang, M. Um, D. Lv, Y. Lu, J. Zhang, Z.-q. Yin, H. Quan, and K. Kim, *Nat. Phys.* **11**, 193 (2015).
 - [31] M. Um, J. Zhang, D. Lv, Y. Lu, S. An, J.-N. Zhang, H. Nha, M. S. Kim, and K. Kim, *Nat. Commun.* **7**, 11410 (2016).
 - [32] M. Demirplak and S. A. Rice, *J. Phys. Chem. A* **107**, 9937 (2003).
 - [33] M. Berry, *J. Phys. A* **42**, 365303 (2009).
 - [34] J. Zhang, J. Zhang, X. Zhang, and K. Kim, *Phys. Rev. A* **89**, 013608 (2014).

- [35] D. M. Meekhof, C. Monroe, B. E. King, W. M. Itano, and D. J. Wineland, *Phys. Rev. Lett.* **76**, 1796 (1996).
- [36] D. Leibfried, R. Blatt, C. Monroe, and D. J. Wineland, *Rev. Mod. Phys.* **75**, 281 (2003).
- [37] H. Häffner, C. F. Roos, and R. Blatt, *Phys. Rep.* **469**, 155 (2008).
- [38] C. Wunderlich, T. Hannemann, T. Körber, H. Häffner, C. Roos, W. Hänsel, R. Blatt, and F. Schmidt-Kaler, *J. Mod. Opt.* **54**, 1541 (2007).
- [39] R. Lechner, C. Maier, C. Hempel, P. Jurcevic, B. P. Lanyon, T. Monz, M. Brownnutt, R. Blatt, and C. F. Roos, *Phys. Rev. A* **93**, 053401 (2016).
- [40] F. Gebert, Y. Wan, F. Wolf, J. C. Heip, and P. O. Schmidt, *New J. Phys.* **18**, 013037 (2016).
- [41] V. Bužek, H. Moya-Cessa, P. L. Knight, and S. J. D. Phoenix, *Phys. Rev. A* **45**, 8190 (1992).
- [42] G. Morigi, E. Solano, B.-G. Englert, and H. Walther, *Phys. Rev. A* **65**, 040102 (2002).
- [43] T. Meunier, S. Gleyzes, P. Maioli, A. Auffeves, G. Nogues, M. Brune, J.-M. Raimond, and S. Haroche, *Phys. Rev. Lett.* **94**, 010401 (2005).
- [44] B. M. Rodriguez-Lara, H. Moya-Cessa, and A. B. Klimov, *Phys. Rev. A* **71**, 023811 (2005).